DOE/ER/03077-226

Courant Mathematics and Computing Laboratory

U.S. Department of Energy

Front Tracking and Two Dimensional Riemann Problems

J. Glimm, C. Klingenberg, O. McBryan,
B. Plohr, D. Sharp, S. Yaniv

Research and Development Report

Supported by the Applied Mathematical Sciences subprogram of the Office of Energy Research, U.S. Department of Energy under Contract DE-AC02-76ER03077

Mathematics and Computers
September 1984

New York University

DOE/ER/03077-226
UC-32
Mathematics and Computers

Courant Mathematics and Computing Laboratory

New York University

FRONT TRACKING AND TWO DIMENSIONAL RIEMANN PROBLEMS

J. Glimm, C. Klingenberg, O. McBryan,
B. Plohr, D. Sharp, and S. Yaniv

September 1984

Supported by the Applied Mathematical Sciences subprogram of the Office of Energy Research, U. S. Department of Energy under Contract No. DE-AC02-76ER03077

DISCLAIMER

Printed in U.S.A.

Available from

National Technical Information Service
U.S. Department of Commerce
5285 Port Royal Road
Springfield, VA 22161

Copy 2.

Table of Contents

FRONT TRACKING AND TWO DIMENSIONAL RIEMANN PROBLEMS

James Glimm [1, 3, 4, 6]
Christian Klingenberg [1, 4]
Oliver McBryan [1, 3, 5, 7]
Bradley Plohr [1, 3]
David Sharp [2, 8]
Sara Yaniv [1, 3, 4]

ABSTRACT

A substantial improvement in resolution has been achieved for the computation of jump discontinuities in gas dynamics using the method of front tracking. The essential feature of this method is that a lower dimensional grid is fitted to and follows the discontinuous waves. At the intersection points of these discontinuities, two-dimensional Riemann problems occur. In this paper we study such two-dimensional Riemann problems from both numerical and theoretical points of view. Specifically included is a numerical solution for the Mach reflection, a general classification scheme for two-dimensional elementary waves, and a discussion of problems and conjectures in this area.

1. Introduction

Many phenomena in nature are modeled by nonlinear hyperbolic systems of conservation laws:

$$u_t + \nabla \cdot \vec{f}(u) = 0 . \tag{1.1}$$

The example considered here is the system of Euler equations for a compressible, inviscid, polytropic gas. The equation (1.1) represents an idealization. Its solutions are the limits, as viscosity parameters tend to zero, of the solutions of more complete equations such as the Navier-Stokes equations. The solutions of interest for the system (1.1) are frequently

1. Courant Institute of Mathematical Sciences, New York University, 251 Mercer Street, New York, N.Y. 10012.
2. Los Alamos National Laboratory, Los Alamos, N.M. 87545.
3. Supported in part by the Applied Mathematical Sciences subprogram of the Office of Energy Research, U.S. Dept. of Energy, Contract DE-AC02-76ERO3077.
4. Supported in part by the Army Research Office, Contract No. DAAG29-83-K-007.
5. Supported in Part by the National Science Foundation, Grant No. MCS-8207965.
6. Supported in part by the National Science Foundation, Grant No. MCS-8243730.
7. Alfred P. Sloan Foundation Fellow.
8. Supported by U.S. Department of Energy.

found to be piecewise smooth. For the Euler equations in one space dimension the jump discontinuities between the smooth pieces are contact discontinuities and shock waves. In two space dimensions these same wave modes give rise to surface singularities of codimension one. The Rankine-Hugoniot conditions, as derived from the integral form of the Euler equations, hold across these jumps.

When solving the system (1.1) numerically, the discontinuities that may occur in its solution may be resolved on coarser grids by the method of front tracking than by conventional finite difference methods. For two space dimensions, front tracking may be described as follows. A one-dimensional grid is placed onto the discontinuity. Its evolution in time is given by a two step procedure, using first the Rankine-Hugoniot relations to propagate the front normally and then using tangential equations to propagate surface waves. This approach works away from the points where the discontinuity curves meet. At such intersection points the geometry does not in general allow an operator splitting into normal and tangential directions, so the evolution of intersection points must be determined as the solution of a two-dimensional Riemann problem. To solve two-dimensional Riemann problems it is crucial to classify the coherent waves, which are defined to be dynamically stable intersection points of one-dimensional coherent waves. The region between the fronts is treated as an initial/boundary-value problem and is solved using (almost) standard finite difference methods. The front and interior schemes are connected in a strip $O(\Delta x)$ in width about the front. For a detailed description see [3].

The front tracking method appears to allow an increase of linear resolution by a factor of three or better, i.e. an improvement in the number of space-time computational grid units by a factor of 27 or better. The method has been tested on various problems. In Sec. 2 and 3 we compare the results of our numerical calculation to experimental results for two specific test problems. An example of how the motion of a two-dimensional coherent wave is determined numerically is given in Sec. 3. In Sec. 4 we show that in two-dimensional compressible gas dynamics there are only a small number of such two-dimensional coherent waves, and in Sec. 5 we conclude with a discussion of outstanding questions related to Riemann problems.

2. Regular Reflection of Shock Waves

The front tracking scheme for two-dimensional gas dynamics has been tested on several problems that admit solution by other means. These problems are: an expanding or contracting circular shock followed by a contact discontinuity, the steady-state supersonic flow past a wedge, the Kelvin-Helmholtz instability, regular reflection of a shock wave, and Mach reflection of a shock wave. For details on the first five see [3].

In this section the numerical solution for nonsteady regular reflection of a shock wave is compared with experimental results [5]. The experiment consists of a planar shock (I) moving down a shock tube and impinging on a wedge with a sufficiently large

angle. When the incident shock strikes the wedge corner a reflected shock (R) is formed, which extends from the reflection point to the shock tube wall, where it forms a bow wave in front of the wedge, as shown in Fig. 2.1. We will refer to the region enclosed by the reflected shock as the "bubble". As with Riemann problems in general, the solution is self-similar, i.e $u(t,\vec{x}) = u(\sigma t,\sigma\vec{x})$ for every $\sigma>0$. In the computation presented here, the Mach number of the incident shock is 2.05 and the angle of the wedge is 63.4°.

The numerical calculation was initialized just after the reflected shock had formed and enclosed only a small region about one quarter of a mesh interval in height. Data at the two ends of the reflected shock were obtained using a shock polar analysis. At the wedge corner, the two velocity components vanish. The remaining solution components at the corner and the full solution in the interior are determined by interpolation. One arbitrary parameter is used in the initialization, which is the oblateness of the bubble, defined as the ratio of the distance of the reflection point from the corner to the distance of the bow shock to the corner (the ratio of the lengths of the segments BC and AB in Fig. 2.1). The initial oblateness was taken from experimental data, but it can be determined approximately by a preliminary calculation because it is constrained to lie in a bounded interval by theoretical considerations. In fact the computational results are quite insensitive to its value. The initialization algorithm can be regarded as an approximate solution of the two-dimensional Riemann problem in a special case.

In Fig. 2.2 the contours of constant density and constant entropy that were obtained numerically are shown. In Fig. 2.3 the density distribution along the wall obtained from the calculation is superimposed on the experimental data.

Further analysis of the solution is possible. Self-similar solutions of the Euler equations satisfy

$$\nabla\cdot(\rho\vec{V}) + \frac{2}{t}\rho = 0, \tag{2.1}$$

$$\vec{V}\times\nabla\left(\tfrac{1}{2}|\vec{V}|^2 + \frac{e+p}{\rho}\right) = T\,\vec{V}\times\nabla S - |\vec{V}|^2\,\nabla\times\vec{V}, \tag{2.2}$$

$$\vec{V}\cdot\nabla\left(\tfrac{1}{2}|\vec{V}|^2 + \frac{e+p}{\rho}\right) + \frac{1}{t}|\vec{V}|^2 = 0, \tag{2.3}$$

and

$$\vec{V}\cdot\nabla S = 0. \tag{2.4}$$

Here ρ is the density, e is the internal energy density, p is the pressure, T is the temperature, S is the entropy, and $\vec{V} = \vec{q} - \vec{x}/t$ is the self-similar velocity, with $\vec{q}$ being the fluid velocity, $\vec{x}$ the position relative to the corner, and t the time elapsed since collision of the shock with the corner. The system is hyperbolic for a flow for which the self-similar velocity is supersonic. For a subsonic self-similar flow, equations (2.1) and (2.2) are elliptic, while equations (2.3) and (2.4) remain hyperbolic. The characteristics

for the hyperbolic modes, viz. the entropy S and the Bernoulli "constant" $\frac{1}{2}|\vec{V}|^2 + (e+p)/\rho$, follow the streamlines (integral curves) of the self-similar velocity $\vec{V}$, which in the weak wave limit can be presumed to vanish only at the wedge corner (where $\vec{x} = 0$ and $\vec{q} = 0$). The entropy is constant along the streamlines of $\vec{V}$, in particular along the walls. Since the entropies behind the reflection point and behind the bow shock differ, the entropy is discontinuous at the wedge corner. Assuming the pressure to be continuous at the corner, it follows that the density is discontinuous there also. This density discontinuity appears to be missing in the experimental picture [5]. Two possible explanations for this discrepancy are (a) that the experiments are not in the weak wave limit and (b) that the density discontinuity is smoothed experimentally by a viscous boundary layer.

We regard the mathematical existence theory for the solution of the regular reflection to be a special case of the Riemann problems discussed in Sec. 5. By the above discussion, we can eliminate the special features of gas dynamics and of the regular reflection geometry to reduce the question to a problem in nonlinear partial differential equations. In fact an existence proof could be organized along the following lines.

For most of its available parameter range, the regular reflection is transonic. The locus of points inside the bubble for which this self-similar velocity is sonic is an arc of a circle that can be determined. The reflected shock is straight where it bounds the supersonic portion of the bubble, and the state in this portion can be computed using shock polars. This is related to, but more elementary than the material discussed in Sec. 3. Thus we take the bubble cut off by the sonic line rather than the full bubble up to the reflection point as the domain under consideration. The corner discontinuity is resolved by the use of polar coordinates r, θ in the plane. On the sonic line the full solution is known, and within the cut off bubble, the solution is subsonic as defined above. The ellipticity is not uniform, however, as the elliptic characteristics become real on the sonic line. There are three portions of the solution: the location of reflected shock bounding the subsonic region, the hyperbolic modes, and the elliptic modes. For the constructive portion of the proof, we propose an iteration on these three portions. During each step, one portion of the solution will be solved, using the other two as data. The estimates on the iteration, which are the key to convergence, are outside the scope of the present discussion.

3. Mach Reflection of Shock Waves

The intersection point of discontinuity curves will be called a node. In a neighborhood of a node the curves are approximated by straight lines separating wedge shaped regions. In analogy with the one-dimensional Riemann problem, we define a two-dimensional Riemann problem to be an initial value problem for a two-dimensional conservation law having data that is either a constant state or a simple rarefaction wave in each of a finite number of wedges. Such problems have been studied for scalar

conservation laws [10,6,7,8], but only special solutions are known for systems of conservation laws. As with the solution of a one-dimensional Riemann problem, the solution of a two-dimensional Riemann problem will evolve into a more complicated configuration containing several elementary waves. Thus in front tracking we must solve a subcase of the full Riemann problem: determining the velocity and states associated with the one specific elementary wave (node) being tracked. We shall report in this section on a method for tracking the Mach node, also called the Mach triple point. Its propagation is a fully two-dimensional problem that cannot be be reduced to one-dimensional problems by spatial operator splitting. In fact successive solutions to one-dimensional problems still play a key role in solution of the Mach triple point, but their composition is governed by the geometry of the waves entering the triple point and not by an orthogonal set of coordinate axes.

Consider a planar shock moving down a shock tube and incident on a wedge with a small angle (see Fig. 3.1). In contrast with the regular reflection case we obtain a Mach reflection. The point where the incident (I) and the reflected shock (R) meet (the "Mach triple point") has lifted off the wall and is connected to the wall by a nearly straight shock called the Mach stem (M). Behind the Mach triple point a contact discontinuity (C) is formed between the reflected shock and the Mach stem.

The corresponding two-dimensional Riemann problem is shown in Fig. 3.2. Because of the Galilean covariance of gas dynamics, any Mach triple point is related by a Galilean transformation to a configuration in which the triple point is stationary, located at the origin, and such that the flow enters the triple point along the positive x-axis. In this rest frame each state is given by the density ρ, the pressure p, and two components of velocity $\vec{q}$, excepting that there is only the x-component of velocity for state 0. The angles at which the waves are oriented in this frame can be determined from the rest-frame states, so the Mach triple point configuration is completely specified once the rest-frame states and the Galilean transformation relating the rest frame and the laboratory frame are known. Given the state in one sector, the Rankine-Hugoniot conditions determine a one-parameter family of states that can occur in a neighboring sector if the two sectors are to be separated by a stationary shock or contact discontinuity. These conditions may be written as follows [4, pp. 301-302 and 329]:

$$\frac{p_i - p_j}{\rho_j} = \vec{q}_j \cdot (\vec{q}_j - \vec{q}_i)$$

for

$$(i,j) \in \{(0,1), (1,0), (1,2), (2,1), (0,3), (3,0)\}, \tag{3.1}$$

$$\frac{p_i}{p_j} = \frac{\mu^2 - \frac{\rho_i}{\rho_j}}{\mu^2 \frac{\rho_i}{\rho_j} - 1}$$

for

$$(i,j) \in \{(1,0), (3,0), (2,1)\}, \tag{3.2}$$

$$\vec{q}_2 \times \vec{q}_3 = 0, \tag{3.3}$$

and

$$p_2 = p_3. \tag{3.4}$$

Here $\mu^2 = \frac{\gamma - 1}{\gamma + 1}$, where γ is the polytropic gas constant. Relations (3.1) and (3.2) are the Rankine-Hugoniot conditions for a shock, while relations (3.3) and (3.4) express the existence of a contact discontinuity.

There are eleven equations for the fifteen rest-frame state variables, and thus four frame-independent or intrinsic parameters needed to specify a Mach triple point in its rest frame. From the point of view of an experimentalist, the initial conditions in a shock tube experiment, viz. three frame independent parameters specifying the density and pressure scales and the strength of the incident shock, are not sufficient to determine the solution. For this reason it could be stated that there is a missing equation for the Mach triple point. However, this missing equation is only an absence of an analytic or closed form solution to give the triple point trajectory on the basis of equations (3.1)−(3.4), and does not indicate an incompleteness of the Cauchy problem for the Euler equations. From a mathematical point of view there is no missing equation, since the solution from the previous time step provides complete Cauchy data.

The front tracking problem is to obtain a complete Riemann problem solution for given Cauchy data and to select the Mach triple point out of that solution. As formulated this problem is too difficult. Hence we proceed with equations (3.1)−(3.4). With fifteen state variables and eleven equations at the triple point, we see that the Mach triple point lies in a four-dimensional manifold within the space of states u_0, u_1, u_2, and u_3. In lieu of solving a full two-dimensional Riemann problem to select a point in this manifold, four of the above fifteen parameters are selected to specify the triple point. Using physical intuition, we selected four parameters from the complete set of Cauchy data. Based on numerical evidence, we believe this method does a satisfactory job of picking out the Mach triple point from the waves emanating from the complete solution of a two-dimensional Riemann problem that is close to a Mach triple point. There are two reasons why the input to the Mach triple point computation may differ from the exact constraints given by equations (3.1)−(3.4) that this elementary wave must satisfy. One is numerical roundoff error, and the other is that signals from the interior influence the states located exactly at the Mach triple point. In the current code, account for this latter aspect is incompletely implemented; future improvements should upgrade both the coupling of the triple point to the interior scheme as well as the selection of the specific triple point out of a general Riemann problem. In the computations presented here the signals propagating from the interior into the Mach triple point are small, as one can see from the

experimental data and setup. In particular the experimental Mach configuration is propagating into an undisturbed ambient region. See also [3] where the same issues are discussed and have been resolved for the propagation of one-dimensional waves (shocks and contacts).

We select the following four parameters: p_0, ρ_0, p_1, p_3. Equations (3.2) give p and ρ in all four sectors at the triple point. Then we solve for the speed $q_0 = \|\vec{q}_0\|$.

The algorithm for finding q_0 is as follows: The jump conditions across each of the three shocks may be reformulated as [4, p. 347]:

$$\tan^2 \theta_j = \left(\frac{\frac{p_i}{p_j} - 1}{\gamma M_j^2 - \frac{p_i}{p_j} + 1} \right)^2 \frac{(1 + \mu^2)(M_j^2 - 1) - \left(\frac{p_i}{p_j} - 1 \right)}{\frac{p_i}{p_j} + \mu^2}$$

for

$$(i,j) \in \{(0,1), (1,2), (0,3)\}, \tag{3.5}$$

where θ_j is the angle that the velocity turns (across a shock) when entering region j and $M = q/c$ is the Mach number, with c, the speed of sound, defined by $c^2 = \gamma p/\rho$. Equations (3.1) may be combined to give

$$q_j^2 = q_i^2 - \left(\frac{1}{\rho_j} + \frac{1}{\rho_i} \right) (p_j - p_i). \tag{3.6}$$

By inserting these relations into (3.5) one obtains expressions for the turning angles in terms of the known densities and pressures and the unknown q_0. Since the flow is parallel to the slip line in states 2 and 3, the following relationship holds between the turning angles:

$$\theta_1 + \theta_2 = \theta_3. \tag{3.7}$$

Solving (3.5) for $\theta_j = \theta_j(q_0)$, $j = 1, 2, 3$, and inserting it into (3.7) we obtain an equation with four possible branches, depending on the signs of the θ_j, $j=2, 3$, or in other words, the sign of the square root coming from (3.5). Note that the turning angle θ_1 across the incident shock is always positive. These four branches are reduced to two branches for the unknown q_0 by squaring:

$$\theta_2^2 - (\theta_1 + |\theta_3|)^2 = 0\,, \quad \theta_3 < 0; \tag{3.8}$$

$$\theta_2^2 - (\theta_1 - |\theta_3|)^2 = 0\,, \quad \theta_3 > 0. \tag{3.9}$$

A solution of equation (3.8) corresponds to negative θ_3 or an inverted Mach triple point [4, p. 335]), while a solution of (3.9) corresponds to positive θ_3 or a direct Mach triple point.

Using numerical experiments we found that equations (3.8) and (3.9) have two roots. For small ratios of p_3 / p_1, the two roots are solutions of equations (3.9), while (3.8) has no roots. For larger values of p_3 / p_1, the larger root is a solution of equation (3.9) and the smaller root is a solution of equation (3.8). Based on numerical evidence, the larger root always corresponds to a positive turning angle θ_2. However for a positive θ_2, the node is actually a degenerate case of the overtake node, as defined in section 4, and probably should not be regarded as a Mach triple point. In the physical experiments we have analyzed [1,2,5] the smaller root represents the physical data. On these two grounds, we selected the smaller root, which is calculated numerically and set equal to q_0.

We define the laboratory frame to be the frame in which the velocity ahead of the incident shock is zero. This frame is further fixed by specifying an angle, for example the direction of propagation of the triple point. We note that the triple point speed in the lab frame equals the rest-frame speed q_0 just determined. Thus the direction of propagation of the triple point can be found geometrically by propagating the incident shock normally in the lab frame for a time Δt (using the Rankine-Hugoniot conditions across the incident shock and the incident shock angle) and intersecting it with a circle of radius $q_0 \Delta t$ centered at the location of the unpropagated triple point. In this way the Galilean transformation from the rest frame to the lab frame is specified, completing the determination of the Mach triple point.

We compared the numerical solution for the nonsteady Mach reflection with experiments in [5]. In the experiment an incident shock with a Mach number 2.03 impinges on a wedge with angle 27°. The calculations were initialized just after the Mach configuration has appeared. The reflected shock and the Mach stem then enclose a region of about one mesh interval in height. After the bubble enclosed a region several mesh intervals in height the solution had settled down to its self-similar form as seen in the experiment. In Fig. 3.3 the constant density contours are shown. In Fig. 3.4 the wall density distribution obtained in our calculation is superimposed on the experimental data. However the calculation is preliminary in two respects. The present form of the algorithm for the propagation of the Mach triple point seems to be stable only when the initial oblateness is chosen near the experimentally determined value. Moreover the algorithm for the propagation of the point of intersection of the contact discontinuity with the wall is discernibly unstable: the fluid velocity at this point is very sensitive to the pressure upstream, so the end of the contact tends to curl up. The causes of these instabilities have not yet been determined.

4. The Classification of Two Dimensional Elementary Waves

In this section we classify the elementary waves for two-dimensional gas dynamics. Front tracking employs a normal and a tangential operator splitting at jump surfaces and a solution of two-dimensional Riemann problems at the point singularities formed by the intersection of jump surfaces ("nodes"). An example of such a two-dimensional Riemann

problem was described in the previous section. In this section we shall show that for two-dimensional compressible gas dynamics there are only a small number of such nodes.

We make some general assumptions that idealize the problem, but which we believe apply to a generic set of possible point singularities formed by the meeting of jump surfaces and centered rarefaction waves. Then we refine these general assumptions into a precise mathematical formulation, and using the latter, derive a classification scheme for the allowed point singularities.

Excluded from this classification scheme are point singularities formed by centered waves (implosions) and points in a neighborhood of which the solution is not piecewise smooth.

Definition 4.1 A *pressure wave* is a shock wave or a centered rarefaction wave. A *wave* is either a pressure wave or a contact discontinuity. A *node* is the point singularity formed by the intersection of waves. A rarefaction wave centered at a node is called an *incoming (forward facing) rarefaction wave* if its straight line C^+ or C^- characteristics, in the frame in which the node is stationary, point towards the node. A shock wave emanating from a node is said to be an *incoming shock wave* if, in the stationary frame, it turns the flow towards the node. Similarly we define an *outgoing rarefaction wave* and an *outgoing shock wave*. We observe that every pressure wave at a node is either incoming or outgoing.

Assumption 4.2. We assume our solution u to be an *elementary wave*, which, in general terms, satisfies the following:

4.2.1 u is a stationary solution of the Euler equations for a polytropic gas: $u_t = 0$ and $\nabla \cdot \vec{f}(u) = 0$;

4.2.2 u has the form

$$u = u_j \text{ for } \theta_{j-1} < \theta < \theta_j, \quad j = 1, \ldots, n$$

where $\theta_n = \theta_0 + 2\pi$ and each u_j is constant or a centered rarefaction wave;

4.2.3 the only jumps allowed in u are shock waves and contact discontinuities;

4.2.4 u is generic;

4.2.5 u is an entropy increasing solution, with

$$u = \lim_{\nu \to 0} \bar{u} ,$$

where $\bar{u}$ is a solution of the Navier-Stokes equations with viscosity ν.

First consider all possible elementary waves containing only contact discontinuities. If one of the sectors has a 180° opening, there can be a nonzero discontinuity in the tangential velocity across its boundary. All other contact discontinuities contain only temperature jumps. It is possible for any number of them to occur, and at any set of angles.

From now on assume that the elementary wave contains at least one pressure wave. Assumptions 4.2.4 and 4.2.5 are not written in mathematical terms, so we formulate the ideas that they express in a manner that we can use in our analysis.

4.2.4a No incoming rarefaction waves are allowed. There can be at most two incoming pressure waves, which are necessarily shock waves. If the flow on the ahead side (the side with the lower pressure) of an incoming shock wave is adjacent to a contact discontinuity that is within 90° of the incoming shock, only this one incoming shock wave is allowed.

4.2.5a No sectors of zero velocity bounded by contact discontinuities ("embedded wedges") are allowed.

Observe that the elementary waves that satisfy 4.2.1 through 4.2.4 but fail to satisfy 4.2.5a can be interpreted as solutions of an initial/boundary-value problem if the contact discontinuities bounding the embedded wedge are replaced with reflecting walls.

Theorem 4.3. There exists a unique streamline through the node.

The proof follows from Propositions 4.6, 4.10, and 4.13 below, in which we show (a) the existence of a streamline entering the node, (b) its uniqueness, and (c) the existence and uniqueness of a streamline leaving the node. We assume that the node is located at the origin.

Lemma 4.4. On each circle centered at the node there exists an open set of points $\vec{x}$ at which the velocity $\vec{q}$ points inward.

Proof. Since the flow is constant in sectors separated by waves, the flow may not be tangential to the circle everywhere. By conservation of mass, velocities pointing out of the circle at some points must be balanced by velocities elsewhere that point inwards.

Lemma 4.5. Suppose a circle centered at the origin is rotated so that an inward-pointing velocity vector $\vec{q}$ from Lemma 4.4 is parallel to the x axis. Then the fluid particles passing through the point $\vec{x}$ of Lemma 4.4 either have passed through an incoming shock (case a) or no wave at all (case b).

Proof. Consider the open sector S that is the smaller of the two sectors bounded by the ray through $\vec{x}$ and the two rays forming the x axis. Consider the wave w in S closest to $\vec{x}$. The wave w may not be a rarefaction wave for the following reason: the C^+ or C^- characteristics of a rarefaction wave in S would form an angle less than 90° with the velocity vector $\vec{q}$, so the rarefaction wave w would be forward facing, which contradicts Assumption 4.2.4a. Neither may w be a contact discontinuity because the flow would not be parallel to it. If w is a shock, it must be an incoming shock since it is oriented at an angle less than 90° with $\vec{q}$.

Proposition 4.6. There exists a streamline entering the node.

Proof. Consider a circle centered at the node together with the velocity vectors based on this circle. Since our solutions are constant along rays, we need only show that there is a vector on this circle that points towards the origin. By Lemma 4.4 there exists

a vector pointing into the circle. By Lemma 4.5 there exists either a streamline entering the node (the x axis in case b) or there exists a neighboring sector closer to the x axis with another vector pointing into the circle (case a). In the latter case we use this new vector pointing inwards to repeat the above argument. Since there are only finitely many sectors, we can find a vector pointing to the origin.

Lemma 4.7. Let S be the smaller of the two open sectors between two streamlines s_1 and s_2 entering the node. There must be at least one wave in S.

Proof. Suppose there were no waves in S. By Assumption 4.2.2, u is constant between waves, so only a constant state with zero velocity would be possible in S. This is ruled out by Assumption 4.2.5a. Thus there must be at least one wave in S.

Lemma 4.8. There cannot be a rarefaction wave in any sector S for which the velocity points towards the node.

Proof. Suppose there were a rarefaction wave w in such a sector S. Since the velocity adjacent to w points into the circle and since the angle between a velocity vector and its C^- and C^- characteristics is less than 90°, the straight line C^+ or C^- characteristics of w would point towards to origin. Then w would be a forward facing rarefaction, which is ruled out by assumption.

Lemma 4.9. There can be no rarefaction wave or contact within an open 90° sector from a streamline s entering a node. The only possible waves in this region are incoming shocks.

Proof. Up to the first wave w_1, from s and within 90° from s, the velocity $\vec{q}$ must be parallel to s and point into the circle. Hence by Lemma 4.8, w_1 may not be a rarefaction wave. Neither can it be a contact discontinuity. It is therefore an incoming shock wave. Since w_1 must turn the flow towards the node, the velocity vectors $\vec{q}$ past w_1, within 90° from s and up to the next wave w_2, also point into the circle and towards s. Repeating the above argument, w_2 must be an incoming shock wave. Thus all of the finitely many waves in an open 90° sector starting at s are incoming shock waves.

Proposition 4.10. The streamline entering the node is unique.

Proof. Suppose there were two streamlines s_1 and s_2 entering the node. Consider the smaller of the two open sectors S bounded by s_1 and s_2. By Lemma 4.7 there must be at least one wave w_1 in S. Since w_1 is within 90° from either s_1 or s_2, w_1 is an incoming shock wave by Lemma 4.9. It is not possible to have constant states with nonzero velocities between s_1 and w_1 and between w_1 and s_2 because the flow directions would be inconsistent along w_1. Thus a second wave w_2 in S is needed, which by Lemma 4.9 must be an incoming shock. Again such a two wave configuration in S is ruled out, which forces a third incoming shock wave. By Assumption 4.2.4a this is ruled out.

We now rotate our coordinates so that the incoming streamline is the positive x axis.

Definition 4.11. We divide the flow through the two-dimensional elementary wave into two components using the unique streamline that enters the node, placed on the positive x axis as follows. Let S^+ be the open set formed by the streamlines starting from $y > 0$, $x = +\infty$ and let S^- be formed from the streamlines starting from $y < 0$, $x = +\infty$.

Lemma 4.12. The closure of $S^+ \cup S^-$ equals the whole plane.

Proof. Suppose this were false. The boundaries of S^+ and S^- are streamlines that are half lines directed into and out of the origin because the solution is constant along rays. Since we know by Propositions 4.6 and 4.10 that there exists a unique streamline entering the node, the two boundaries of S^- and S^+ ahead of the node coincide with the positive x axis. Behind the node they bound an open sector R. Place a circle C around the node. Since the velocity is parallel to the boundaries of S^+ and S^- there is no mass flux through the sides of R. Hence the total flux across $R \cap C$ equals zero. It is not possible that all states within R have zero velocity because of Assumption 4.2.5a. Thus suppose some state within R has nonzero velocity. Since the total flux across $R \cap C$ is zero, the velocity must enter the circle C at some point in R. By Lemma 4.5 and the proof of Proposition 4.6, this implies that there is a streamline in R that enters the node. This is not possible by Proposition 4.10. Consequently R is empty.

Proposition 4.13. The streamline leaving the node is unique.

Proof. By Lemma 4.12 the streamline entering and leaving the node is contained in the boundary between S^+ or S^- and thus exists and is unique.

Lemma 4.14. It is not possible for a single streamline to pass through two consecutive outgoing pressure waves.

Proof. This is based on the following facts: in the coordinates normal and tangential to a stationary shock, the normal component of the velocity is greater than the sound speed in front of a shock and less than the sound speed behind. In the coordinates normal and tangential to the straight line C^+ or C^- characteristics of a stationary rarefaction wave, the normal component of the velocity is equal to the sound speed. We now rule out two successive shocks; the other cases are similar. Suppose a streamline passes through two outgoing shocks. Then behind the first shock the normal component of velocity with respect to this first shock is less than the sound speed in that sector. Now consider the same velocity vector with respect to the second shock (see Fig. 4.1). Since both shocks are outgoing and the flow passes through them consecutively, the normal component with respect to the second shock is smaller than that component with respect to the first shock. Hence the normal component of velocity is less than the sound speed in front of the second shock, contradicting the above mentioned fact of gas dynamics.

Corollary 4.15. There is at most one rarefaction wave.

Proof. Assume that there are two rarefaction waves. By assumption 4.2.4a a rarefaction wave may not be incoming and thus by the Lemma 4.14 there is at most one

rarefaction wave in S^+ and at most one in S^-. A rarefaction turns the flow counterclockwise if it lies in S^+ and clockwise if it lies in S^-. Since the flow is already turned in these directions by incoming shock waves, if there are any, and since there are no other pressure waves that might turn the flow in the reverse direction, this flow configuration is not possible.

Corollary 4.16. There must be at least one incoming shock wave in the region $x > 0$.

Proof. Suppose there are no incoming shock waves in $x > 0$. Then there are no pressure waves at all in this region. The region $x < 0$ is divided into two sectors by the outgoing streamline. In each of these sectors there may be at most one pressure wave. Thus we have the following possibilities:

a) Two shocks, Fig. 4.2. This configuration forces us to introduce an embedded wedge, which is ruled out by hypothesis.

b) One shock, one rarefaction, Fig. 4.3. Here the pressure increases through the shock but decreases through the rarefaction wave, leaving a pressure jump that cannot be maintained across a contact discontinuity along the outgoing streamline.

c) A single rarefaction wave or shock is clearly not possible.

To recapitulate, we have determined that an elementary wave is restricted by the following. There is a unique streamline through the node. There is either one or two incoming shock waves. There is no more than one outgoing pressure wave on each side of the streamline leaving the node, only one of which may be a rarefaction. The streamline is a contact discontinuity if there are two outgoing pressure waves. This then leaves us with only a small number of possible elementary waves, which we shall determine presently.

Theorem 4.17. Under Assumptions 4.2 an elementary wave containing at least one pressure wave is one of the following types, as specified in detail below: cross, overtake, Mach, diffraction, and transmission.

Proof. Case 1. (Diffraction or transmission) Suppose the streamline entering the node is a contact discontinuity. Then by assumption 4.2.4a there may be at most one entering shock; all the other waves must be outgoing. By Corollary 4.16 there must be exactly one incoming shock. We say that this incoming shock impinges or is incident on the contact discontinuity. Any additional waves lie only in the region that allows for outgoing shocks or rarefaction waves. Consider the shaded region in Fig. 4.4. This shaded region is divided into two sectors ("outgoing sectors") by the outgoing streamline. By Lemma 4.16 there may be at most one pressure wave in each of the outgoing sectors. This then allows for the following possible combination of waves in the outgoing sectors:

a) Two shocks, Fig. 4.5.a. This is a possible solution. It is the diffraction of a shock impinging on a contact discontinuity, causing a reflected and a transmitted shock. We show in Fig. 4.5.b how the solution may be constructed by drawing the appropriate shock

polars in the θ, p plane.

b) One shock, one rarefaction wave. The configuration in Fig. 4.6.a is an elementary wave. It is as in Fig. 4.5.a, but with a rarefaction wave in place of a reflected shock. The solution is constructed using shock polars, as indicated in Fig. 4.6.b. On the other hand, the configuration in Fig. 4.7 is not possible since the pressure increases across the two shocks but decreases across the rarefaction wave, so that the pressures cannot match.

c) A single shock. A shock incident on a contact discontinuity causing a reflected shock with no transmitted wave (see Fig. 4.8) is not allowed since the presures do not match. A shock impinging on a contact discontinuity and causing a transmitted shock but no reflected wave (see Fig. 4.9.a) is a possible elementary wave; see the corresponding shock polar in Fig. 4.9.b.

d) A single rarefaction wave. A shock incident on a contact discontinuity causing a reflected rarefaction wave but no transmitted wave, as in Fig. 4.10, is not allowed. Since a rarefaction wave turns the flow further in the same direction as the shock does, one would obtain a sector smaller than 180° of zero velocity that would be bounded by contact discontinuities. This is ruled out by Assumption 4.2.5a. A shock incident on a contact discontinuity causing a transmitted rarefaction wave but no reflected wave (see Fig. 4.11) is not possible since the pressures would not match behind the waves.

Case 2. (Mach node) Suppose the incoming streamline is not a contact discontinuity. Then by Corollary 4.16 there must be at least one incoming shock and by Assumption 4.2.4a there may be at most two. Suppose there is only one incoming shock. Then there may be only one pressure wave in each of the two outgoing sectors, which allows for the following possibilities:

a) Two shocks. A direct Mach reflection, where the incident shock breaks into two shocks, the reflected shock and the Mach stem, is a possible elementary wave; see Fig 4.12.a. The solution is found using shock polars as in Fig 4.12.b.

The parameter space here, consisting of the state at $x = +\infty$ and the shock strength of the incident shock, is on the boundary of the parameter space of the case to be considered in Fig. 4.18 where two incident shocks collide. Thus setting the strength of the second incident shock to zero gives this elementary wave.

b) One shock, one rarefaction. The configuration in Fig. 4.13, where an incoming shock breaks up into a reflected rarefaction wave and a "Mach stem", is not possible, as can be seen by setting the shock polar O equal to the shock polar O' in Fig. 4.6.b. It is not possible to connect two points in the supersonic region on the right branch of a shock polar by the image of a $\Gamma-$characteristic that decreases pressure and increases the turning angle. The configuration shown in Fig. 4.14, where an incoming shock breaks up into a reflected shock and a rarefaction wave, is not possible, for the pressures cannot match behind the node.

c) A single outgoing shock or rarefaction is not possible.

Case 3. Now consider the case of two incoming shocks. There are two possibilities:

Case 3A. (Overtake) The flow passes through both incoming shocks consecutively. We have the following possible configurations in the outgoing sectors:

a) Two shocks. It is possible to have two incoming shocks overtake each other and give rise to two outgoing shocks separated by a contact discontinuity (see Fig. 4.15.a). The solution may be constructed using shock polars as in Fig. 4.15.b. The special case where one of the two incoming shocks has zero strength coincides with the Mach node case 2a). Also the special case where the reflected shock behind the two incoming waves has zero strength is possible; it is similar to a Mach node, except that the reflected shock is replaced by a second incident shock.

b) One shock, one reflected rarefaction wave. One shock may overtake the other, resulting in a reflected rarefaction and a transmitted shock (see Fig 4.16.a). This possibility is a solution. The solution is found using shock polars as in Fig. 4.16.b. Note that for the same parameters of the two incident shocks, both this case and the previous case are possible. The configuration of Fig. 4.17, in which the flow in S^+ passes through three shocks, and the flow in S^- passes only through a simple rarefaction wave, is not possible, since the pressures do not match.

c) A single outgoing shock or rarefaction wave is not possible.

Case 3B. (Cross or Mach node) It is also possible for the two incoming shocks to be on opposite sides of the incoming streamline. Then the possible nodes are:

a) Two incident shocks colliding to form two reflected shocks separated by a streamline (see Fig. 4.18.a) is a possible elementary wave. The solution is found using shock polars as in Fig. 4.18.b. The special case of one incident shock having zero strength gives the direct Mach node of case 2a).

b) We did not determine theoretically whether it is possible for two shocks to cross and to form a reflected rarefaction wave together with a reflected shock, as shown in Fig. 4.19, but on the basis of numerical evidence it appears that this node is not possible.

c) One rarefaction wave in the outgoing sector is not possible. A single shock wave in the outgoing sector defines the inverted Mach node; this interaction is a limit of case a) above, where the shock between region 2 and 3 in Fig. 4.18.a reduces to zero.

5. Some Problems and Conjectures Concerning Riemann Problems

In this section we drop the restriction to two dimensions and to gas dynamics, but we retain the terminology of Sec. 4. Recall that in steady supersonic two-dimensional gas dynamics, where the direction of the flow defines a timelike direction, the equations can be reduced to the form of a one-dimensional time-dependent system of conservation laws. Then the two-dimensional elementary waves viewed in the stationary frame are Riemann problems for a distinct but related one-dimensional system. Similarly Riemann problem

solutions in $n-1$ space dimensions are qualitatively similar to elementary waves in n dimensions.

We list some problems of general interest in this area.

1. The possible n-dimensional elementary waves for a system of conservation laws could be classified. The elementary waves in two-dimensional polytropic gas dynamics were classified in the previous section.

2. Let the incoming wave operator be the solution operator bringing two or more elementary waves to a single point and thereby defining a Riemann problem. The incoming wave operator also acts on single elementary waves by mapping to the configuration at a time of bifurcation, or dynamic instability; this also defines a Riemann problem. The range of this operator is limited to the possible mergers or bifurcations of the elementary waves found in the classification above. Can this range be categorized?

3. The outgoing wave operator gives the possible elementary waves that may occur in the solution of the Riemann problems in the range of the incoming wave operator. We pose the question of existence of solutions for this restricted set of data. Are solutions piecewise smooth, so that there is a finite number of outgoing elementary waves? The answer depends on the order of the system, the dimension of space, and the convexity or number of inflection points in the flux function, as examples [7] indicate and analogies [9] suggest.

4. A logical scattering matrix S is a map from sets of incoming wave types to sets of outgoing wave types as labeled by the solutions to problem 1. It decides which types of incoming waves produce which types of outgoing waves. In the language of quantum mechanics, the problem here is to classify the possible S matrix graphs. Let us consider this problem from the point of view of two-dimensional gas dynamics. We restrict attention to Riemann data contained in the range of the incoming wave operator as defined in 2 above. Under such restriction, the waves will be said to be in incoming order. The allowed nodes of Sec. 4 provide interchange of wave order to an outgoing order. In general, however, the interchange of wave order produces three outgoing waves from two incoming waves and need not reduce the total number of wave pairs that fail to be in outgoing order. On this basis, we expect that even simple incoming configurations could produce complicated outgoing wave interactions. It is possible that the complication (e.g. the number of nodes), while not bounded *a priori*, is still finite. In fact the wave interactions typically decrease the Mach number of the flow, and may give rise to a subsonic region, inside of which no pressure waves can occur. Related to this possibility is the occurrence of nodes with only two outgoing waves. Such nodes allow the interchange of wave order with a reduction in the total number of pairs that are out of order.

5. Uniqueness is an open problem. Well known problems of nonuniqueness are not understood on a fundamental level. For example, consider an incident shock hitting a wedge, resulting in either a regular reflection or Mach reflection. There are regions

where both solutions are possible. By introducing additional physical effects such as viscosity, with a resulting boundary layer, or surface roughness on a certain length scale, this overlapping region of nonuniqueness might disappear.

6. Extended or nonlocal Riemann problems may be considered, where the restriction of constancy in sectors between the waves is replaced by linear or higher order data. This has been implemented for one dimension in the normal propagation of the front [3].

7. Lower order terms in the equations and new waves in the Riemann solution may be caused by geometrical effects and by external sources.

8. The geometry in the large defined on the state space by the flux function needs to be understood. For gas dynamics the qualitative behavior of solutions may be studied by considering the acoustic waves of the linearized problem. But this is not the case for all hyperbolic conservation laws, and new families of waves may be possible in the large. The topology defined by the critical points of the flux function $\vec{f}$ in (1.1) is important here. A critical point is a point in state space where the gradient $A = \nabla \vec{f}$ has coinciding eigenvalues. At the critical points equation (1.1) is no longer strictly hyperbolic; moreover A can fail to have a complete set of eigenvectors. Such a loss of strict hyperbolicity is not pathological in applications, and the mathematical consequences of this fact have not been developed. An extension of this phenomena are the problems for which the equations in different regions of state space change type. The applications are of general interest: oil reservoir simulation, transonic flow in gas dynamics, chemically reacting flows, and nonlinear elasticity.

Acknowledgements

We thank Jonathan Goodman for helpful discussions.

References

1. G. Ben-Dor, "Regions and Transitions of Nonstationary Oblique Shock-Wave Diffractions in Perfect and Imperfect Gases," Report No. 232, UTIAS, 1978.
2. G. Ben-Dor and I. Glass, "Nonstationary Oblique Shock-Wave Reflections: Actual Isopycnics and Numerical Experiments," *AIAA Journal*, vol. 16, pp. 1146-1153, (1978).
3. I-L. Chern, J. Glimm, O. McBryan, B. Plohr, and S. Yaniv, "Front Tracking for Gas Dynamics," *Submitted to J. Comp. Physics*, 1984.
4. R. Courant and K. Friedrichs, *Supersonic Flow and Shock Waves*, Interscience, New York, 1948.
5. R. Deschambault and I. Glass, "An Update On Non-Stationary Oblique Shock-Wave Reflections:," *J. Fluid Mech.*, vol. 131, pp. 27-57, (1983).

6. J. Guckenheimer, "Shocks and Rarefactions in Two Space Dimensions," *Arch. Rational Mech. Anal.*, vol. 59, pp. 281-291, (1975).

7. B. Lindquist, "The Scalar Riemann Problem in One and Two Spatial Dimensions: Piecewise Smooth Solutions," NYU Preprint, 1984.

8. B. Lindquist, "Construction of Two Dimensional Riemann Problems," NYU Preprint, 1984.

9. J. Rauch and M. Reed, "Jump Discontinuities of Semilinear, Strictly Hyperbolic Systems in Two Variables," *Comm. Math. Physics*, vol. 81, pp. 203-227, (1981).

10. D. Wagner, "The Riemann Problem in Two Space Dimensions for a Single Conservation Law," *J. Math. Anal.*, vol. 14, pp. 534-559, SIAM J. Math. Anal., (1983).

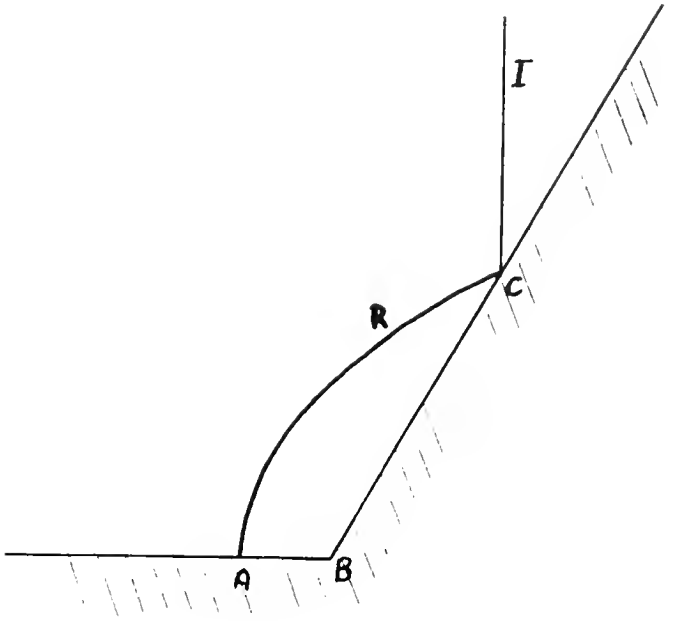

Fig. 2.1. Regular reflection of a shock wave by a wedge. A vertical shock *I* has struck a 63° wedge from the left, causing a reflected shock *R*, which forms a bowshock in front of the wedge.

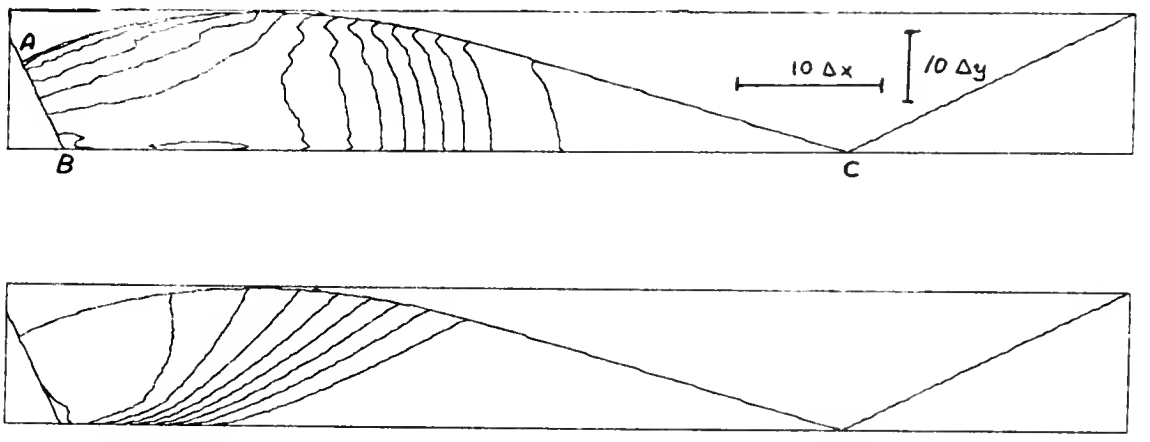

Fig. 2.2. The numerical simulation of a regular reflection, where the incident shock has Mach number 2.05 and the wedge angle is 63.4°. The calculation was performed on a 80 by 20 grid. The top picture shows the lines of constant density inside the bubble formed by the reflected shock. The bottom picture shows the lines of constant entropy. They should coincide with the integral curves for the self-similar velocity field. Theoretical arguments in the text suggest that these integral curves all terminate at the corner.

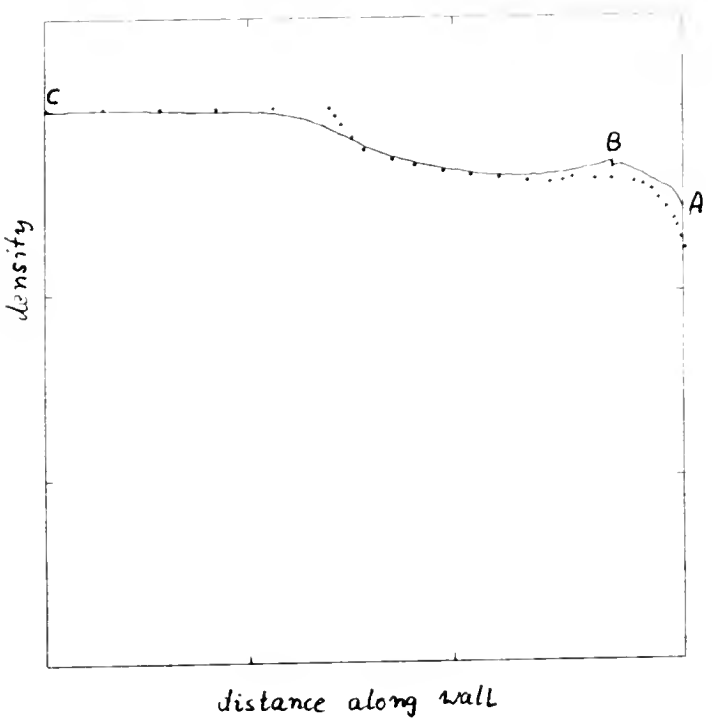

Fig. 2.3. The computed (solid line) density distribution along the wall for the regular reflection run compared to the data obtained in the experiments of Deschambault and Glass (dots).

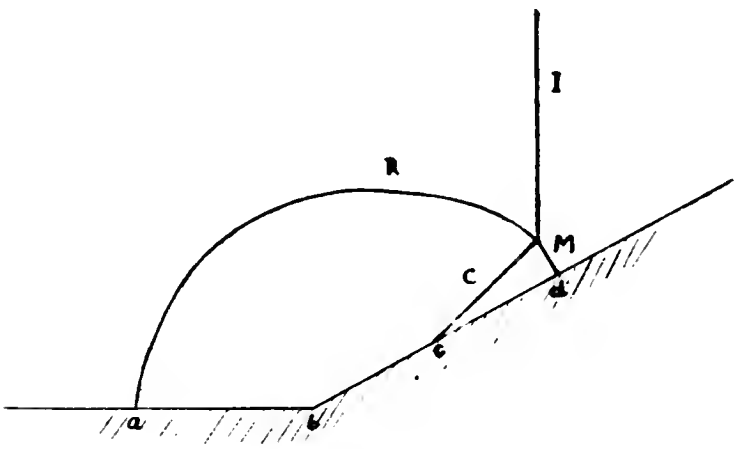

Fig. 3.1. Mach reflection of a shock wave by a wedge. A vertical shock *I* has struck a 27° wedge from the left. The point where the incident shock *I* and reflected shock *R* meet is connected to the wall by a shock called a Mach stem (*M*). Behind the triple point, where the three shocks meet, a contact discontinuity *C* is formed between the reflected shock and the Mach stem.

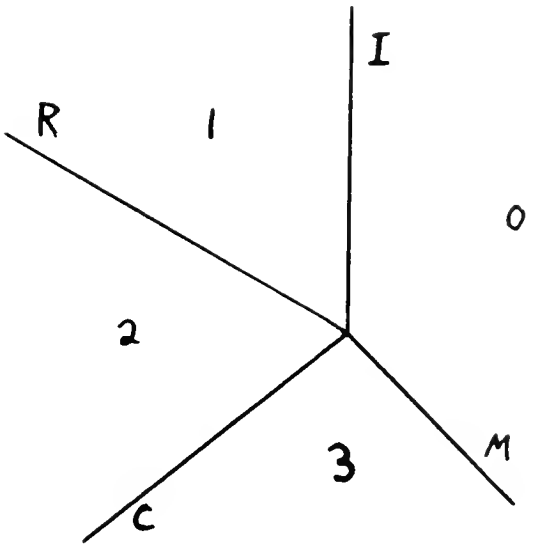

Fig. 3.2. The Riemann problem corresponding to the triple point obtained in a Mach reflection. We assume the shocks and contact discontinuities are straight lines (labeled as in Fig. 3.1) with constant states 0 through 3 in the wedges.

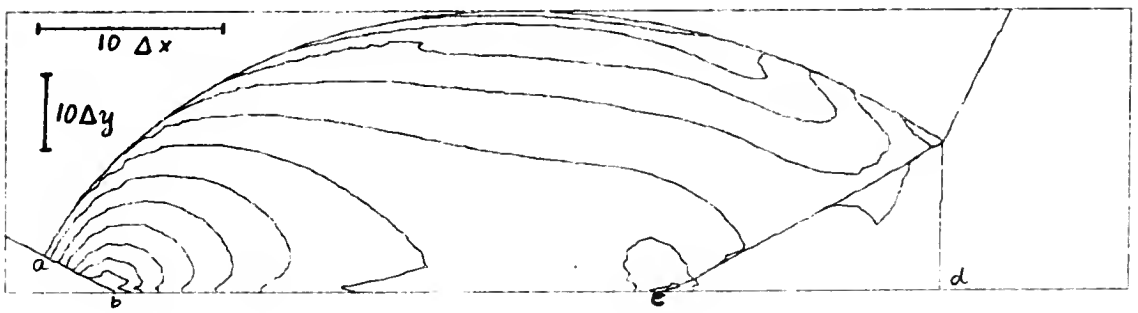

Fig. 3.3. The numerical simulation of a Mach reflection, where the incident shock has Mach number 2.03 and the wedge angle is 27°. Inside the bubble formed by the reflected shock we show the calculated lines of constant density. The calculations were performed on a 60 by 40 grid.

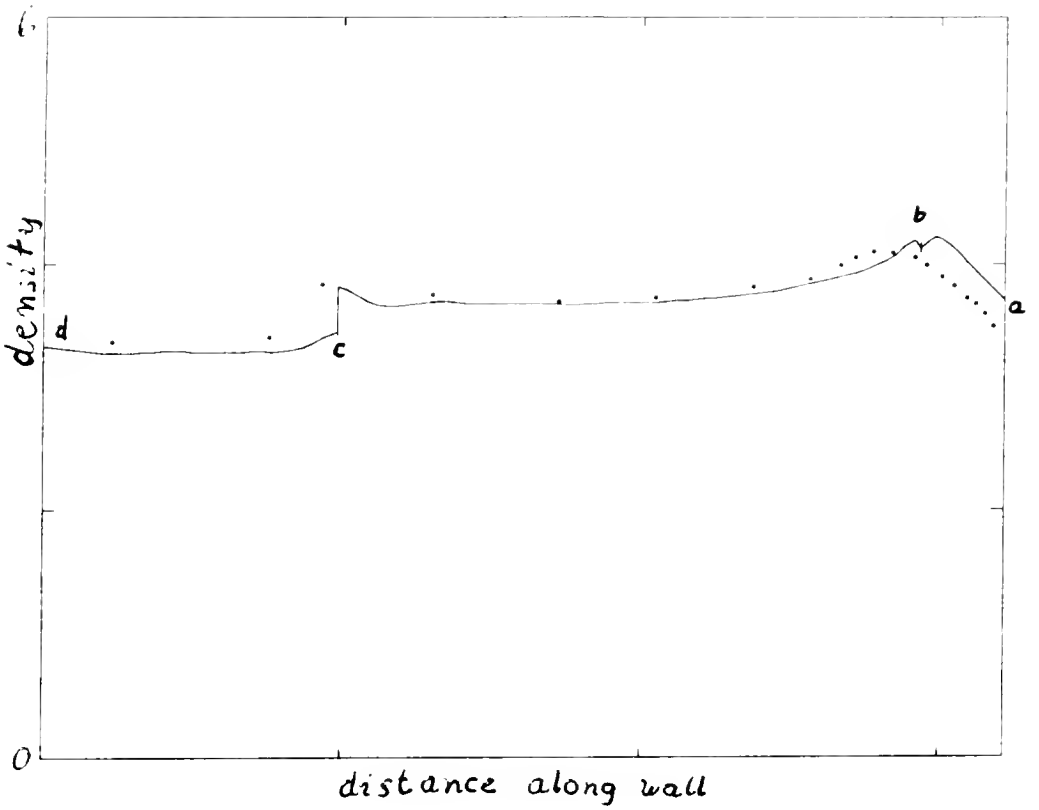

Fig. 3.4. The density distribution along the wall of the Mach reflection run (solid line) shown superimposed on the data found experimentally by Deschambault and Glass (dots).

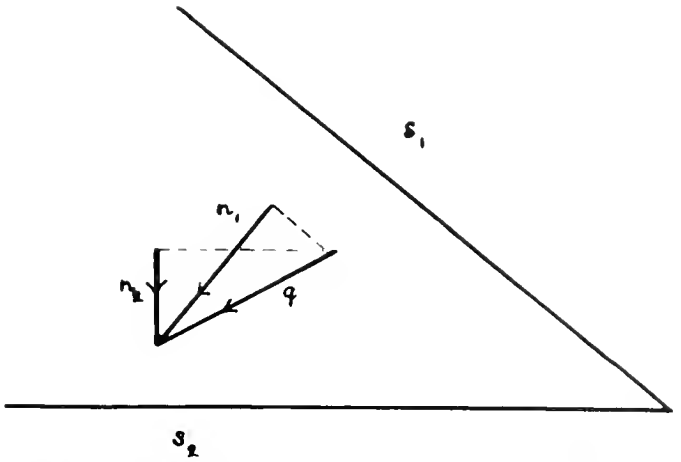

Fig. 4.1. A streamline passing consecutively through two outgoing shocks s_1 and s_2. Both shocks turn the flow away from the intersection point of s_1 and s_2. This is an impossible configuration, as shown in Lemma 4.14. Here $\vec{q}$ is the velocity vector in the sector between s_1 and s_2 and $\vec{n}_i$ is the normal component of $\vec{q}$ with respect to s_i, $i = 1,2$.

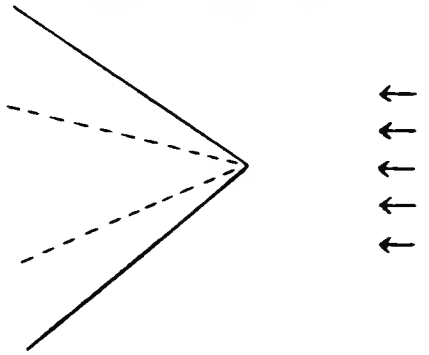

Fig. 4.2. Excluded. A configuration with only two shocks leaving the intersection point is impossible. The smaller of the two sectors between them contains a wedge of zero velocity bounded by contact discontinuities, which is ruled out by Assumption 4.2.5a.

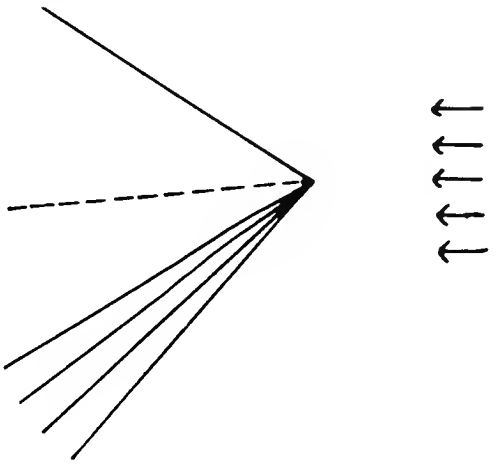

Fig. 4.3. Excluded. It is not possible to have only one shock and one rarefaction wave leaving their point of intersection because the pressures would not match.

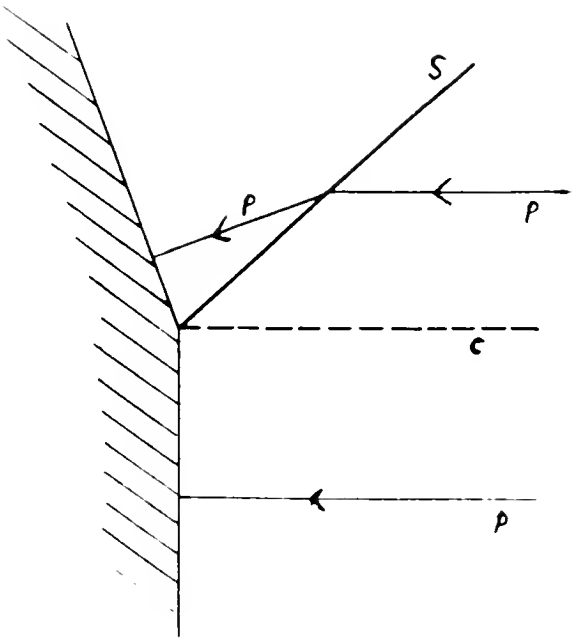

Fig. 4.4. An incident shock *I* impinging on a contact discontinuity *C*. Two particle paths *P* are shown. Outgoing shock and rarefaction waves are allowed only in the shaded region.

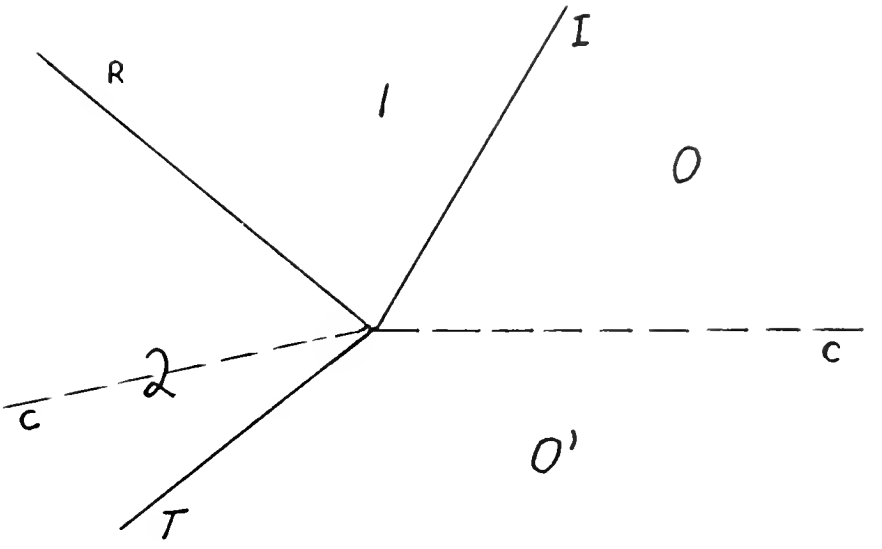

Fig. 4.5.a. Diffraction. A shock *I* can diffract through a contact discontinuity *C* to cause a reflected shock *R* and a transmitted shock *T*.

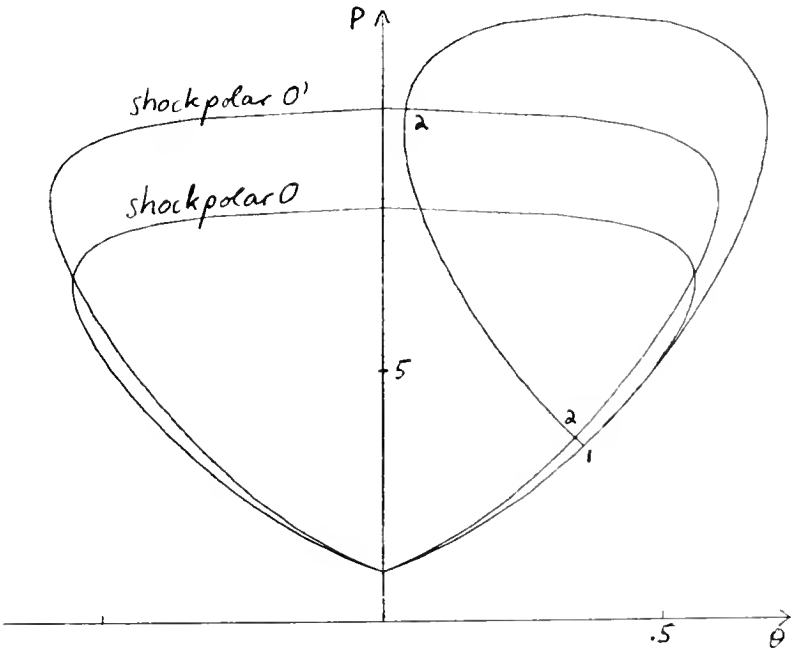

Fig. 4.5.b. The shock polars corresponding to Fig. 4.5.a. The Mach number of state 0 is 2.7 and that of state 0' is 3. The shock strength of *I* is 3.

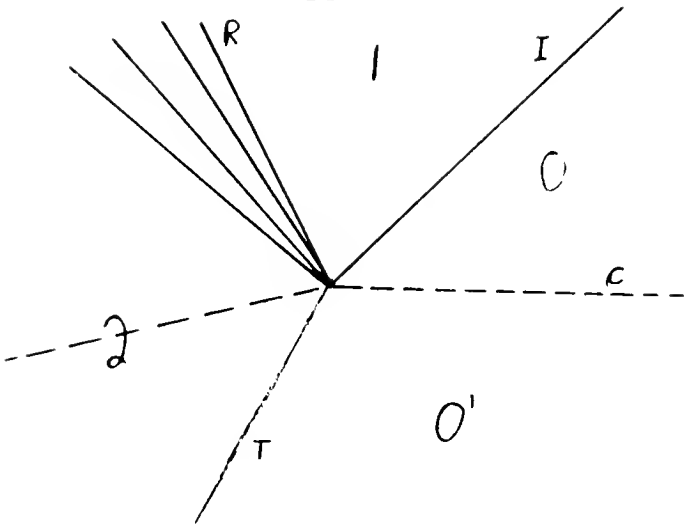

Fig. 4.6.a. Diffraction. The diffraction of a shock I by a contact discontinuity C can cause a reflected rarefaction wave R and a transmitted shock T.

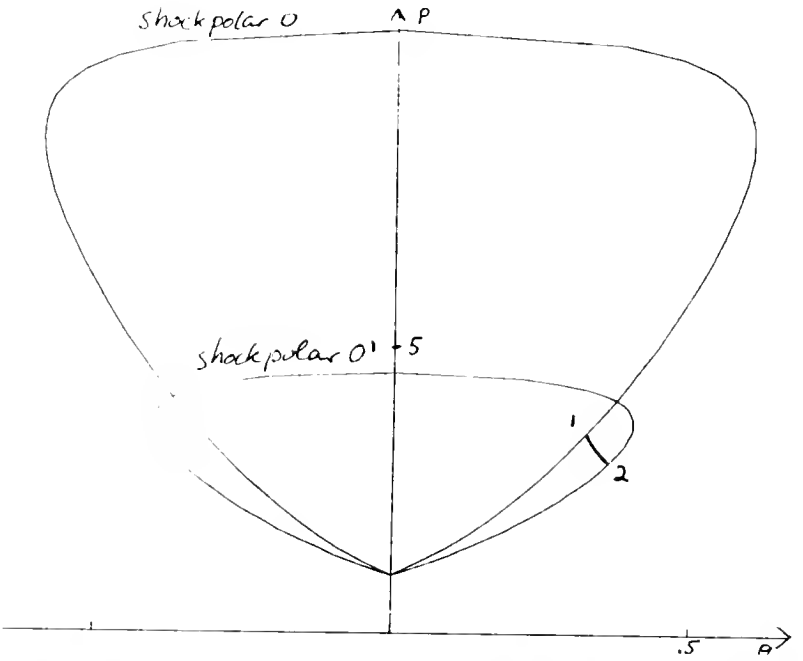

Fig. 4.6.b. The shock polars corresponding to Fig. 4.6.a. The Mach number of state 0 is 3 and that of state 0′ is 2. The image of a $\Gamma-$characteristic in this p , θ plane is drawn, connecting the states $p = 3$ on one shock polar to $p = 2.8$ on the other.

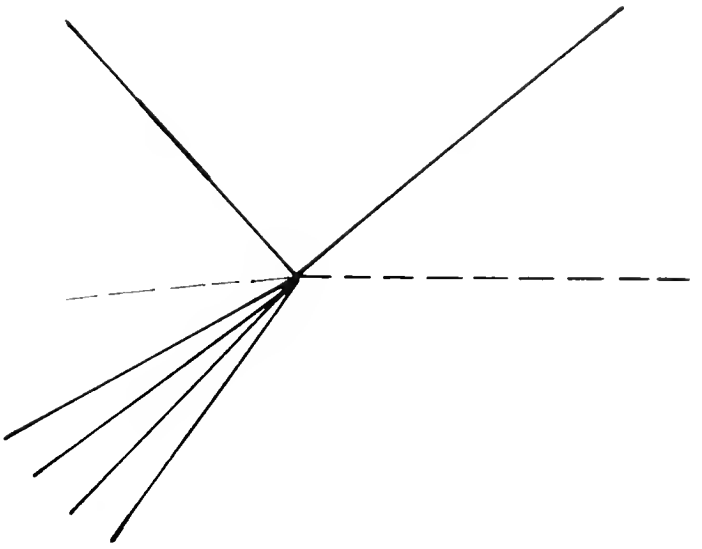

Fig. 4.7. Excluded. A shock incident on a contact discontinuity causing a reflected shock and a transmitted rarefaction wave is not possible since the pressures would not match.

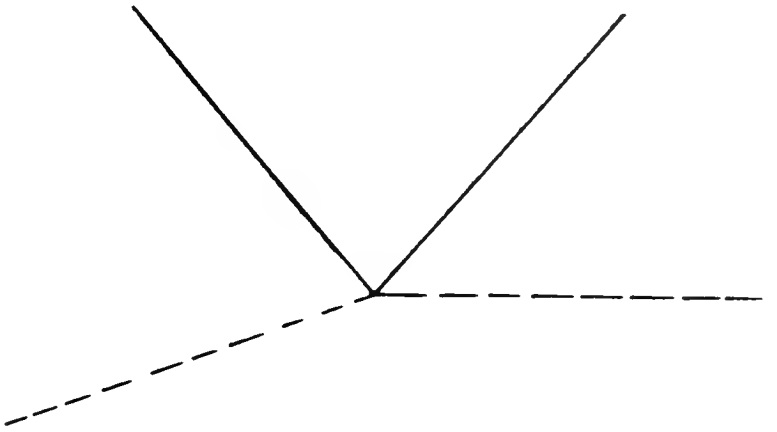

Fig. 4.8. Excluded. A shock incident on a contact discontinuity causing a reflected shock but no transmitted wave is ruled out since the pressures would not match.

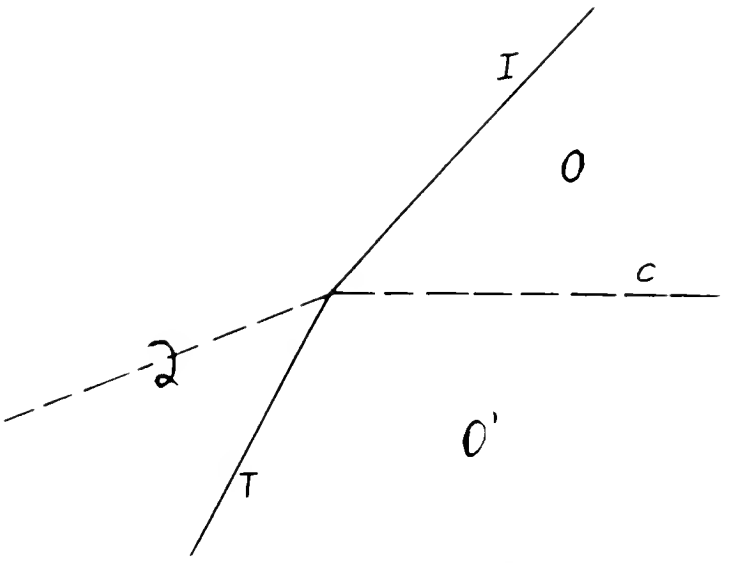

Fig. 4.9.a. Transmission. A shock *I* incident on a contact discontinuity *C* causing a transmitted shock *T* but no reflected wave is possible.

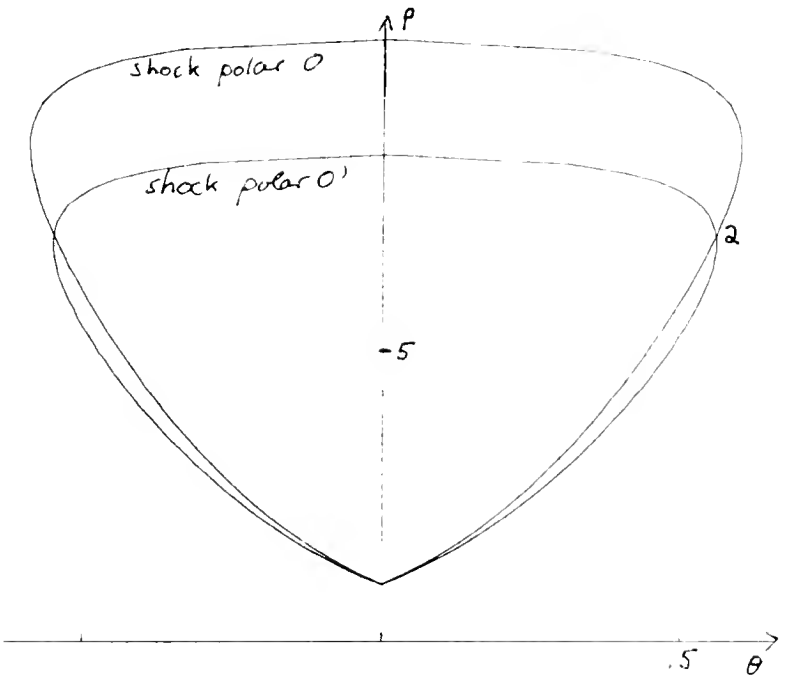

Fig. 4.9.b. The shock polars corresponding to Fig. 4.9.a. The Mach number of state 0 is 3 and that of state 0′ is 2.7.

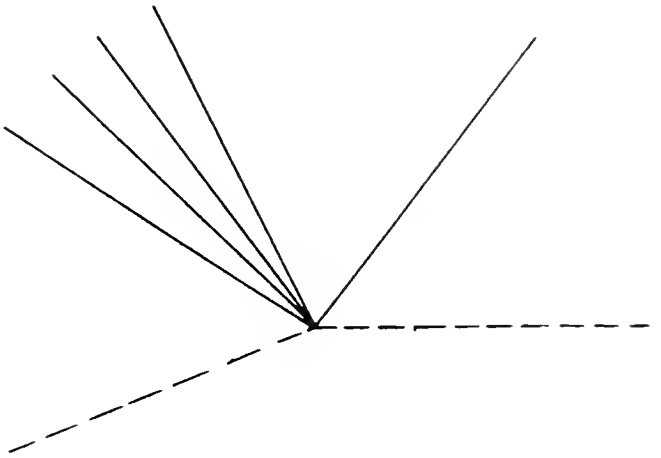

Fig. 4.10. Excluded. A shock incident on a contact discontinuity causing only a reflected rarefaction wave and no transmitted wave is not possible. The rarefaction wave would turn the flow in the same direction as the shock does, thus causing a sector smaller than 180° of zero velocity bounded by contact discontinuities. This is ruled out by Assumption 4.2.5a.

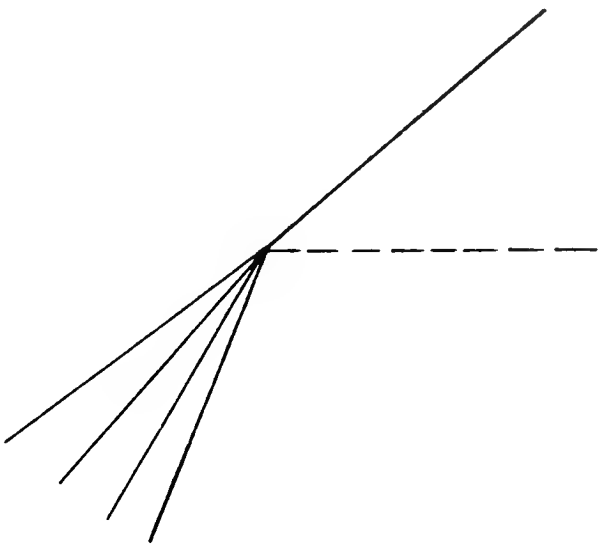

Fig. 4.11. Excluded. A shock incident on a contact discontinuity causing a transmitted rarefaction wave but no reflected wave is not possible since the pressures would not match.

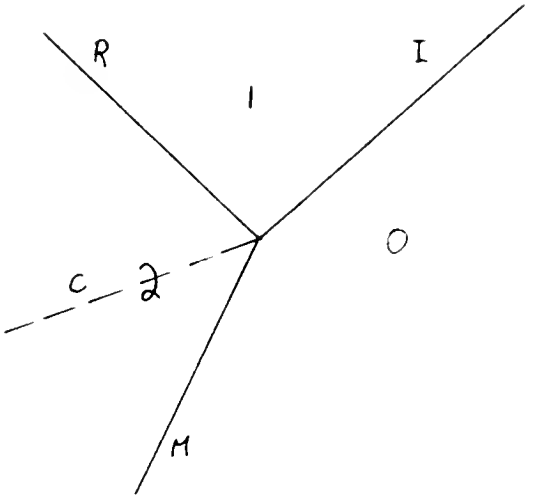

Fig. 4.12.a. Mach node. Direct Mach reflection is shown, with the incident shock *I* breaking into a reflected shock *R* and a Mach stem *M* separated by a contact discontinuity *C*.

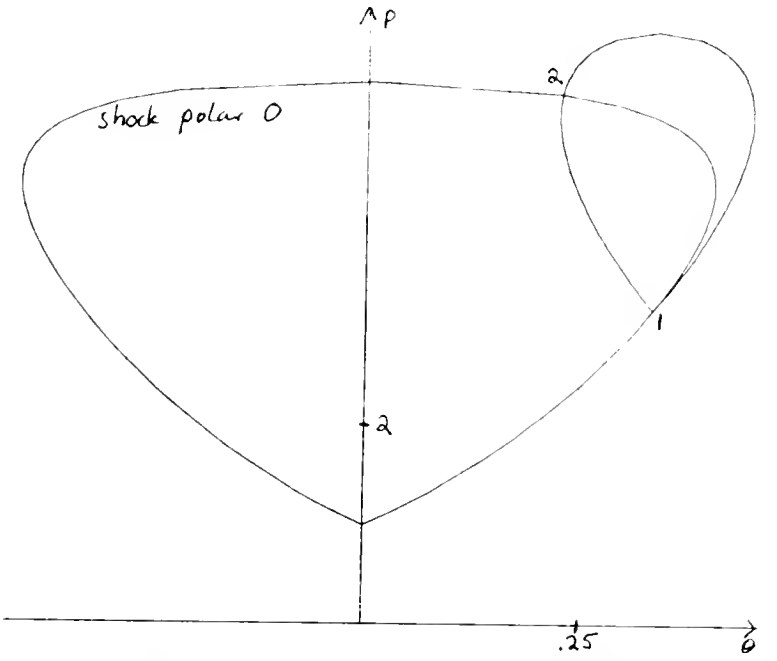

Fig. 4.12.b. The shock polars corresponding to Fig. 4.12a. The Mach number of state 0 is 2.2 and the shock strength of *I* is 3.2.

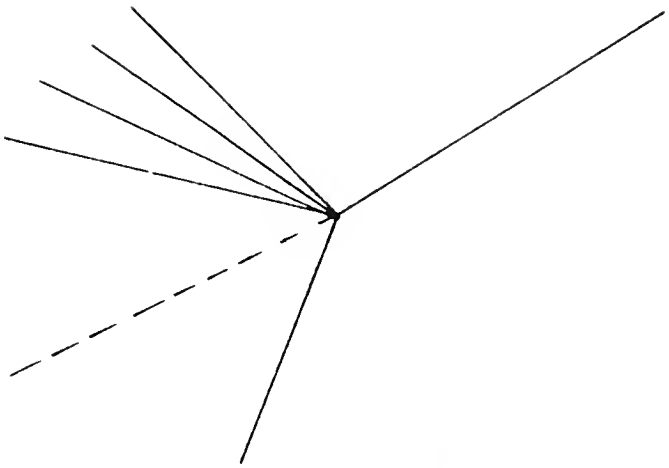

Fig. 4.13. Excluded. It is not possible to have a rarefaction wave instead of the reflected shock in the Mach configuration of Fig. 4.12.a. Behind the two outgoing waves the flow would be inconsistent.

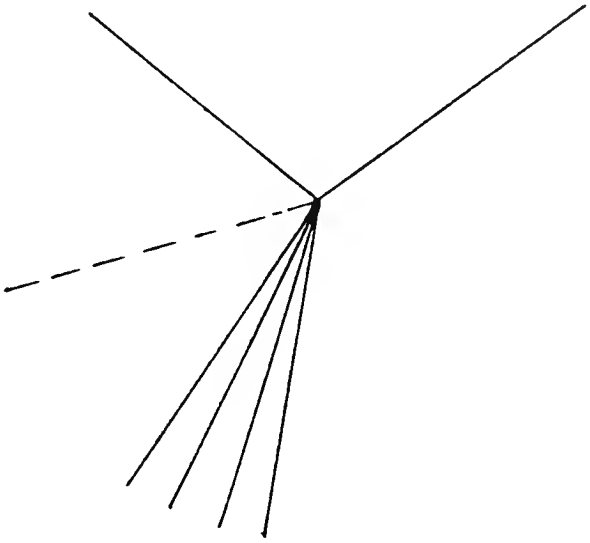

Fig. 4.14. Excluded. It is not possible to substitute a rarefaction wave for the Mach stem in Fig. 4.12.a. The pressures would not match.

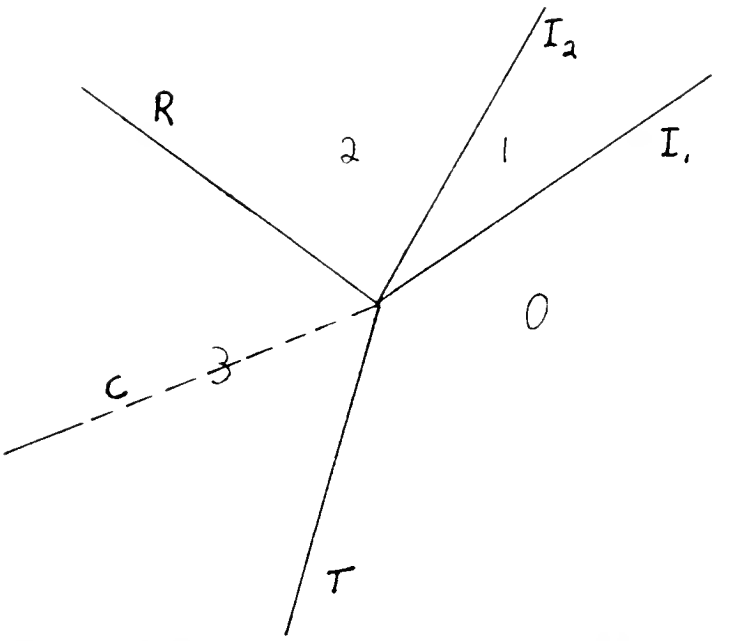

Fig. 4.15.a. Overtake. It is possible to have one incoming shock I_1 overtake another I_2 to cause a reflected shock R and a transmitted shock T with a contact discontinuity C between them.

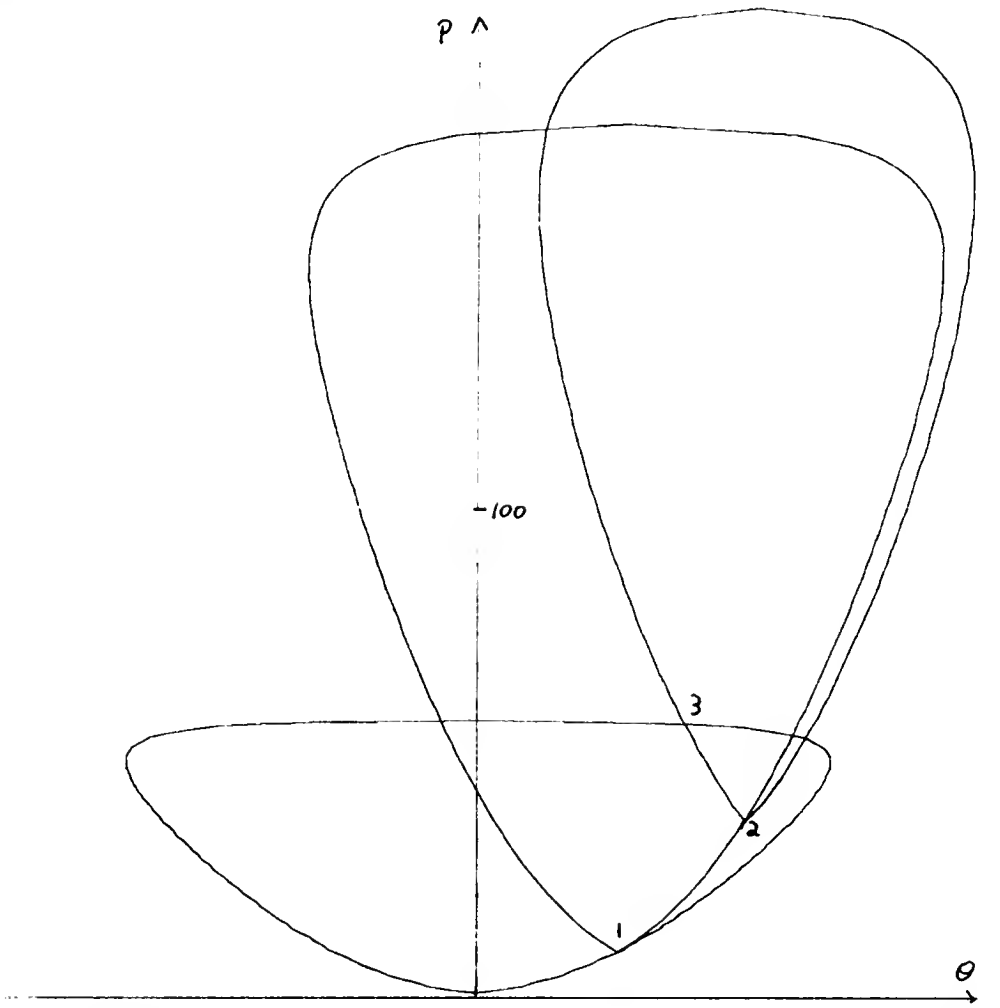

Fig. 4.15.b. The shock polars corresponding to Fig. 4.15.a. The Mach number of state 0 is 7, the shock strength of the incident shock I_1 is 9.5, and the shock strength of I_2 is 3.9.

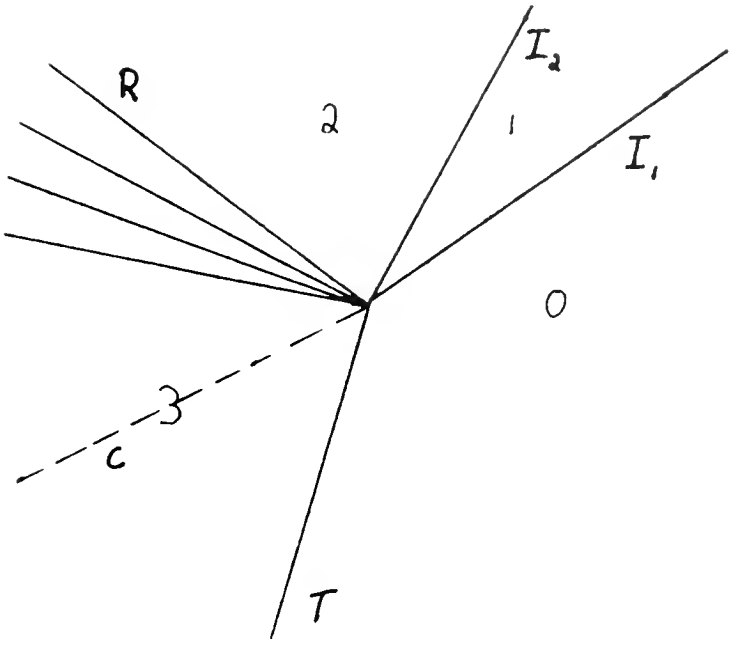

Fig. 4.16.a. Overtake. It is possible for one incoming shock I_1 to overtake another I_2 to cause a reflected rarefaction wave and a transmitted shock wave separated by a contact discontinuity.

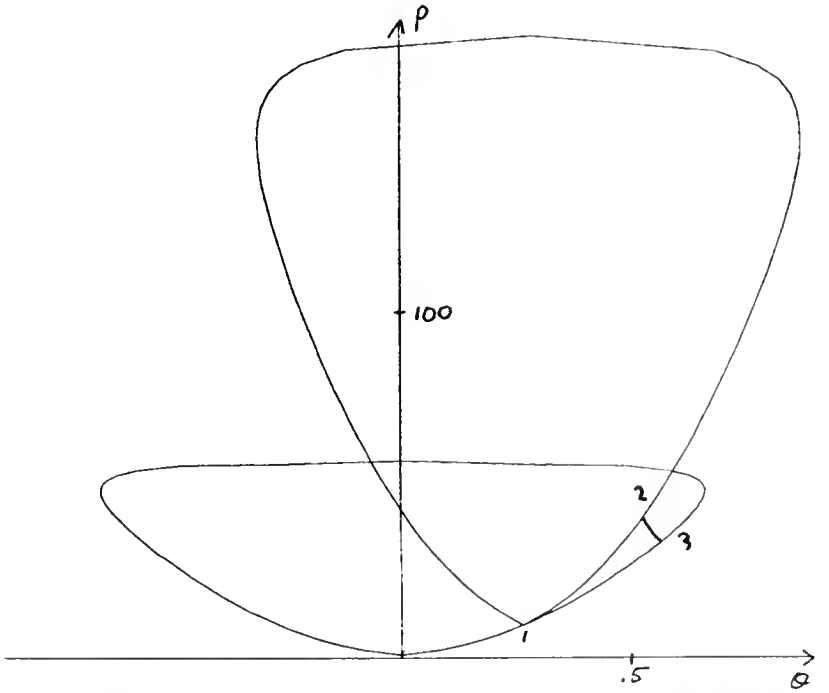

Fig. 4.16.b. The shock polars corresponding to Fig. 4.16.a. The Mach number of state 0 is 7, the shock strength of the incident shock I_1 is 9.5, and the shock strength of I_2 is 3.9.

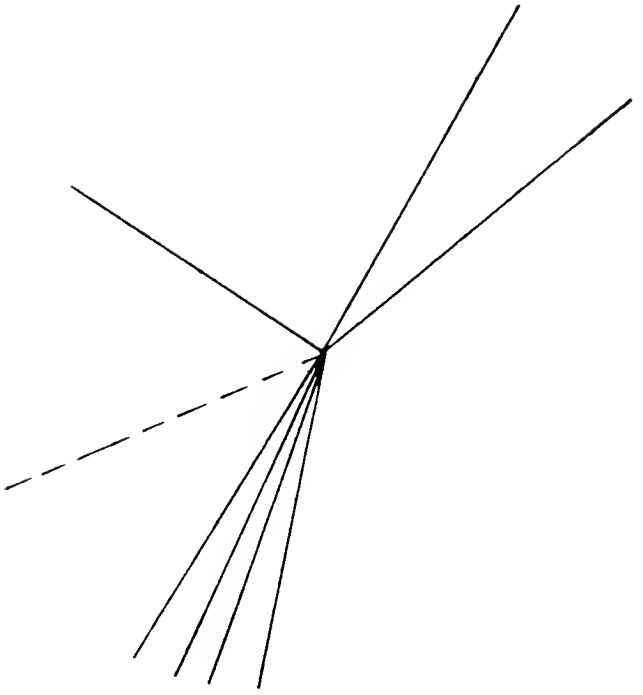

Fig. 4.17. Excluded. It is impossible to have one half of the flow cross only shocks and the other half cross only a rarefaction wave because the pressures would not match.

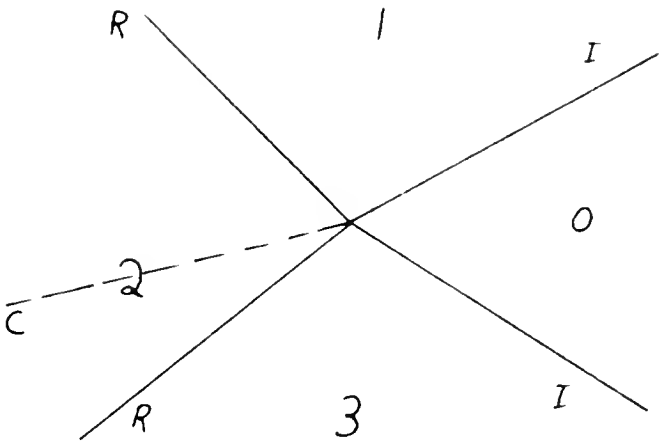

Fig. 4.18.a. Cross. Two may shocks collide and cause two reflected shocks separated by a contact discontinuity.

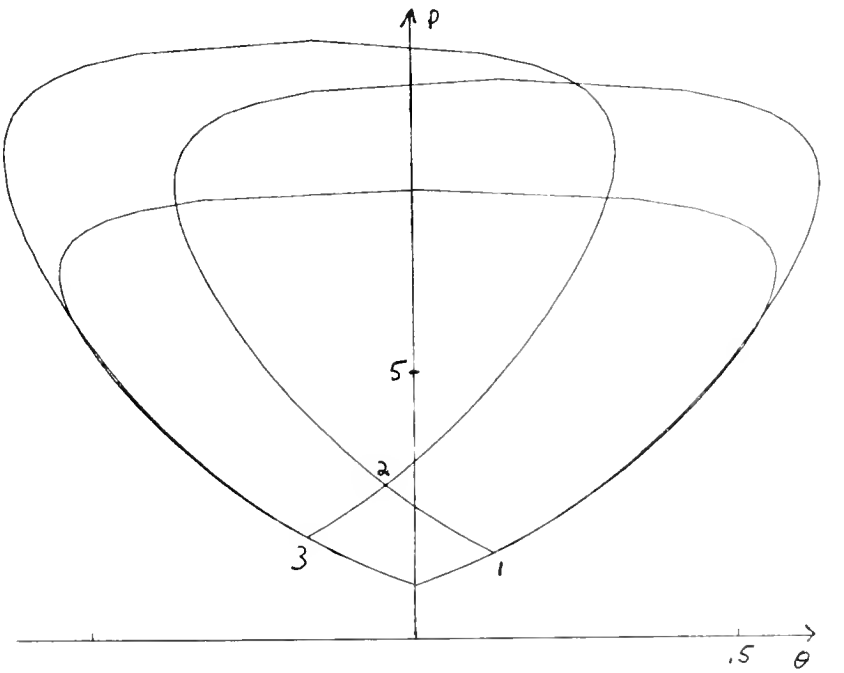

Fig. 4.18.b. The shock polars corresponding to Fig. 4.18.a. The Mach number of state 0 is 2.7 and the shock strengths of the incident shocks are 1.6 and 1.9.

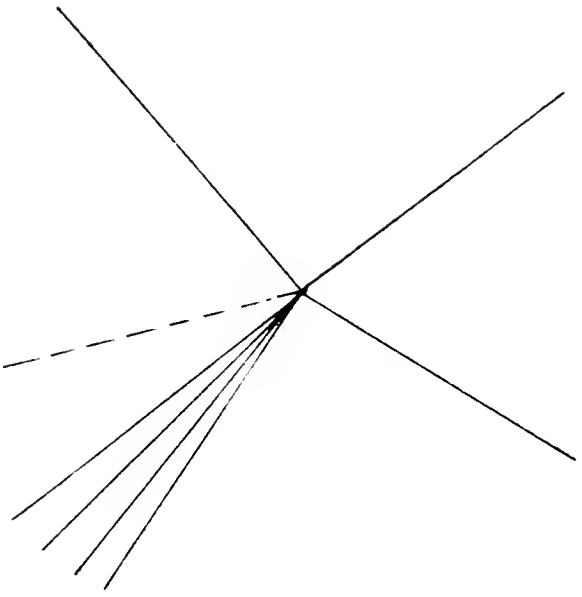

Fig. 4.19. Undecided. Based on numerical evidence it appears to be impossible to substitute a rarefaction wave for the reflected shock in Fig. 4.18.a.